Unexpected link between an antibiotic, pannexin channels, and apoptosis

Ivan K. H. Poon[1,2,3,5], **Yu-Hsin Chiu**[4], **Allison J. Armstrong**[1,2,3], **Jason M. Kinchen**[1,2,3], **Ignacio J. Juncadella**[1,2,3], **Douglas A. Bayliss**[4], and **Kodi S. Ravichandran**[1,2,3]

[1]The Center for Cell Clearance, University of Virginia, Charlottesville, Virginia 22908, USA

[2]Department of Microbiology, University of Virginia, Charlottesville, Virginia 22908, USA

[3]Beirne B. Carter Center for Immunology Research, University of Virginia, Charlottesville, Virginia 22908, USA

[4]Department of Pharmacology, University of Virginia, Charlottesville, Virginia 22908, USA

[5]La Trobe Institute for Molecular Science, La Trobe University, Melbourne, Victoria 3086, Australia

Abstract

Plasma membrane pannexin 1 channels (PANX1) release nucleotide find-me signals from apoptotic cells to attract phagocytes. In a small molecule screen, we discovered the quinolone antibiotic trovafloxacin as a novel PANX1 inhibitor. Although quinolones are widely used to treat bacterial infections, some quinolones have unexplained side effects, including deaths among children. PANX1 is a direct target of trovafloxacin at drug concentrations seen in human plasma, and its inhibition led to dysregulated fragmentation of apoptotic cells. Genetic loss of PANX1 phenocopied trovafloxacin effects, revealing a non-redundant role for pannexin channels in regulating cellular disassembly during apoptosis. Increase in drug-resistant bacteria worldwide and the dearth of new antibiotics is a major human health challenge. Comparing different quinolone antibiotics suggests that certain structural features may contribute to PANX1 blockade. These data identify a novel linkage between an antibiotic, pannexin channels, and cellular integrity, and suggest that re-engineering certain quinolones might help develop newer antibacterials.

Pannexins are four-pass transmembrane channels identified as a new family of channels for small molecules (up to ~1kDa) across the plasma membrane[1,2]. Among the three vertebrate pannexin family members (PANX1, PANX2 and PANX3), PANX1 is the most widely

expressed[1], and implicated in regulating neutrophil activation[3], airway inflammation[4], HIV infection[5], vasoconstriction[6], migraine[7] and other neurological disorders[8,9]. This broad and diverse range of functions may in part arise from pannexin channel-mediated release of purines such as ATP into the extracellular space, where purinergic signaling can influence multiple physiological processes[10,11]. Thus, PANX1 is an attractive therapeutic target for human diseases and we sought to identify small molecules that can modulate PANX1 function.

Caspase-mediated cleavage of PANX1 C-terminus during apoptosis leads to PANX1 channel opening and release of nucleotide find-me signals from early apoptotic cells to recruit phagocytes[12-14,15] (Fig. 1a). This channel opening also allows the entry of fluorescent dyes including TO-PRO-3[13,15] (Fig. 1a). We optimized TO-PRO3 uptake by apoptotic Jurkat cells as a reliable, medium-throughput, flow cytometry-based assay for monitoring PANX1 activity. We tested a 'library of pharmacologically active compounds' (LOPAC[1280TM]) containing 1280 small molecules targeting a diverse range of cellular processes – including currently marketed drugs, failed candidates, and bioactive molecules with known activities. The initial screen revealed three potential PANX1 inhibitors that were tested in secondary screens. Among them, trovafloxacin (a quinolone-based antibiotic) was identified as a potent inhibitor of TO-PRO-3 uptake by apoptotic cells (Fig. 1b). The use of trovafloxacin in patients has been linked to serious adverse side effects, including effects on the central nervous system, hepatic toxicity and in some cases mortality, but the molecular target(s) of trovafloxacin in mammalian cells is unclear[16,17]. Trovafloxacin inhibition of PANX1 was dose-dependent, and comparable to the known pannexin inhibitor carbenoxolone (CBX) (Fig. 1c). Trovafloxacin also inhibited ATP release from apoptotic cells (Fig. 1d). Importantly, trovafloxacin did not inhibit caspase 3/7 activation, or caspase-mediated PANX1 cleavage during apoptosis (Extended Data Fig. 1a,b), ruling these out as reasons.

Several additional analyses suggested trovafloxacin could directly target PANX1 channel activity. Adding trovafloxacin to cells already undergoing apoptosis (i.e. with open PANX1 channels) acutely blocked TO-PRO-3 uptake (Extended Data Fig. 1c,d). When we measured apoptosis-induced plasma membrane PANX1 currents at the single-cell level, via whole-cell patch-clamp recordings, trovafloxacin rapidly inhibited the inward current (at -50mV), with minimal effect on outward current (at +80mV) (Fig. 1e and Extended Data Fig. 1e). We have previously shown that the C-terminal tail of PANX1 blocks the channel pore, and that adding excess soluble C-terminal tails can inhibit 'open' PANX1 channels, especially the inward current (analogous to trovafloxacin)[14]. In contrast, CBX blocked both inward and outward currents[13, 18, 19] (Fig. 1e,f). Trovafloxacin did not inhibit connexin 43 gap junction or PANX2 (Extended Data Fig. 1f-i). Using a TEV-protease system to cleave the C-terminal tail of recombinant PANX1 and induce channel activity (independent of apoptosis)[13,14], trovafloxacin again potently blocked open PANX1 channels (Fig. 1g). To test direct channel blocking, we recorded TEV-cleaved PANX1 single channel activity in excised inside-out patch clamp by adding trovafloxacin to the patch; this led to an increase in the time spent in the closed state, with open probability (NPo) of ~0.85 in control conditions reduced to ~0.15 with trovafloxacin (Fig. 1h). The half maximal inhibitory concentration (IC$_{50}$) of trovafloxacin was ~4μM for the PANX1 inward current (Fig. 1i), similar to concentrations

normally achieved in human plasma (2-10μM)[20,21]. These data suggested that mammalian PANX1 channels could be a direct target of antibiotic trovafloxacin.

Next, we investigated trovafloxacin effects on apoptotic cells via microscopy and made several surprising observations. Besides reducing TO-PRO-3 uptake by apoptotic cells, trovafloxacin also induced the formation of smaller particles; these 'fragments of apoptotic cells' were annexin V[+] indicating phosphatidylserine exposure, and resembled apoptotic bodies that arise after cell disassembly during apoptosis[22,23] (Fig. 2a,b). To quantitate these apoptotic bodies, we designed a flow cytometry-based assay (Extended Data Fig. 2a,b) to simultaneously analyze five parameters: cell size (forward scatter, FSC), cellular complexity (side scatter, SSC), annexin V staining (indicating apoptosis), TO-PRO-3 uptake (PANX1 opening), and 7-AAD staining (loss of plasma membrane integrity). We also performed ImageStream analysis, which combines flow cytometry and image acquisition to confirm the categorization of cells and apoptotic bodies (Extended Data Fig. 2c). The apoptotic bodies were annexin V[intermediate] (compared to annexin V^{high} apoptotic cells), with smaller size and reduced complexity (Extended Data Fig. 2). Trovafloxacin promoted the formation of apoptotic bodies in a concentration-dependent manner (Fig. 2c,d). Importantly, without an apoptotic stimulus, trovafloxacin did not induce apoptosis or apoptotic bodies (Extended Data Fig. 1a), suggesting that trovafloxacin likely modulates steps during apoptosis that promote cellular disassembly. Although trovafloxacin itself did not induce apoptosis, since the human body turns over >200 billion cells daily via apoptosis as part of homeostasis[24], trovafloxacin could impact these apoptotic steps.

While some studies have addressed apoptotic cell disassembly, the mechanisms that control the formation of apoptotic bodies are not well understood[22,23,25,26]. Several lines of evidence suggested a key role for PANX1 in regulating apoptotic cell integrity/disassembly. First, blocking pannexin channels in apoptotic Jurkat cells with CBX or probenecid (another pannexin inhibitor[27]) promoted formation of apoptotic bodies (Fig. 2e,f). Second, this effect was not dependent on the mode of apoptosis induction, as blocking PANX1 during Fas- or UV-mediated apoptosis promoted formation of apoptotic bodies (Fig. 2f and Extended Data Fig. 3a). Third, using loss of cellular complexity during apoptosis as an indication of fragmentation of larger apoptotic cells (SSC[high]/higher cellular complexity) into smaller apoptotic bodies (SSC[low]/lower cellular complexity), blocking PANX1 reduced the SSC[high] particles (Fig. 2g). Treating wild-type primary thymocytes undergoing apoptosis *ex vivo* with trovafloxacin, CBX or probenecid also led to more apoptotic bodies with reduced cellular complexity (Fig. 3a,b). Fourth, the enhanced apoptotic bodies correlated inversely with TO-PRO-3 uptake (Extended Data Fig. 3b), with progressively more PANX1 channel blocking leading to greater formation of apoptotic bodies. Fifth, in a genetic approach, overexpressing a dominant negative form of PANX1 (PANX1 DN) with a mutant caspase cleavage site that can interfere with endogenous PANX1 function[13] (Extended Data Fig. 4a) resulted in increased formation of apoptotic bodies (Fig. 2h). Conversely, overexpressing wild-type PANX1 (PANX1 WT) led to fewer apoptotic bodies. This 'gain of function' due to PANX1 WT expression was still dependent on PANX1 channel activity, with reversal by PANX1 blockers (Fig. 2i). Lastly, blocking PANX1 channel functions did not affect some known apoptotic features such as DNA fragmentation (Extended Data Fig. 4b) or

phosphatidylserine exposure (Fig. 2b). Collectively, these data identify PANX1 as a regulator of cellular disassembly during apoptosis.

To address how trovafloxacin and PANX1 might affect apoptosis in a whole animal, we used intraperitoneal dexamethasone injection to induce synchronous apoptosis of a large fraction of mouse thymocytes *in vivo*[12,28] (Fig. 3c). Administering trovafloxacin with dexamethasone promoted the fragmentation of the apoptotic thymocytes (Fig. 3d, with reduced SSC[high] particles; see Extended Data Fig. 5 and 6 for gating strategy). However, in these experiments we could not track thymic trovafloxacin concentrations, and trovafloxacin *in vivo* could also have had other effects beyond PANX1. Therefore, we generated mice carrying deletion of *Panx1*, using embryonic stem cells engineered to disrupt the *Panx1* gene (Extended Data Fig. 7). In the thymus of Panx1^{-/-} and Panx1^{+/-} mice treated with dexamethasone, the fragmentation of apoptotic cells was enhanced (Fig. 3e), essentially phenocopying the effect of trovafloxacin treatment in wild-type mice (Fig. 3d). The apoptotic particles from *Panx1*^{-/-} and *Panx1*^{+/-} mice also showed reduced TO-PRO-3 uptake (Fig. 3e). To rule out that loss of PANX1 in other tissues contributed to the observed thymic phenotypes in the global knockout mice, we specifically deleted *Panx1* in thymocytes by crossing the *Panx1*^{fl/fl} mice with Lck-Cre mice, where Cre is expressed in the T cell lineage (Extended Data Fig. 7). Similar apoptotic fragmentation and loss of TO-PRO-3 uptake were observed when PANX1 was deleted specifically in thymocytes (Fig. 3f), suggesting a cell autonomous effect. *Ex vivo*, apoptotic thymocytes from PANX1 global knockout mice or the Lck-Cre/*Panx1*^{fl/fl} mice also showed enhanced formation of apoptotic bodies, decreased TO-PRO-3 uptake, and reduced cellular complexity (Fig. 3g-i). Collectively, these data suggest that PANX1 critically influences cellular integrity of dying cells, with loss of PANX1 function either genetically or via trovafloxacin treatment promoting disassembly of apoptotic cells.

One possible mechanism for this increased cellular fragmentation is the lack of ATP that would normally be released by apoptotic cells, and the various autocrine and paracrine signaling via P2 purinergic receptors[3,5,12,13,29]. However, adding exogenous ATP to apoptotic cells when PANX1 channel activity was blocked did not inhibit apoptotic bodies formation (Extended Data Fig. 3c,d). Conversely, adding recombinant apyrase (to hydrolyze ATP) during induction of apoptosis did not promote the formation of apoptotic bodies (Extended Data Fig. 3e). Furthermore, treatment with suramin, a broad inhibitor of P2 family G-protein-coupled receptors, did not enhance formation of apoptotic bodies (Extended Data Fig. 3f). Thus, the extracellular ATP levels and P2 purinergic receptor signaling are not likely directly involved in regulating apoptotic cell integrity.

We next used time-lapse microscopy to monitor cell morphology and TO-PRO-3 uptake. In our experimental conditions with Jurkat cells induced to undergo Fas-mediated apoptosis, most cells begin to show rounding and membrane blebs around 60-90 minutes, and continue to bleb for another 30-60 minutes, a time period referred here as 'dynamic blebbing'. Remarkably, very few of these blebs detach from the apoptotic cell, and after cessation of the dynamic blebbing, these blebs remain attached to the dying cell (Fig. 4a,b and Supplementary video 1). When we added TO-PRO-3 into the medium and tracked its uptake as a measure of PANX1 activity, TO-PRO-3 staining was detected prior to cell rounding and

the onset of blebbing (Fig. 4c and Extended Data Fig. 4c). This suggests that PANX1 channels are activated/opened prior to detection of membrane blebbing.

When we compared cells with normal or impaired PANX1 function (treated with trovafloxacin or CBX, or expressing PANX1 DN mutant), a previously unappreciated step during dynamic membrane blebbing regulated by pannexin channels was revealed. Specifically, apoptotic cells with impaired PANX1 function produced long string-like structures, which we preliminarily denote 'apoptopodia', with blebs of different sizes attached to the ends (Fig. 4a,b,d and Supplementary video 2 and 3). These apoptopodia were annexin V[+], indicating phosphatidylserine exposure (Fig. 4e). While few apoptopodia were seen in apoptotic cells with normal PANX1 function, their frequency was substantially enhanced by blocking PANX1 (Fig. 4f). Blocking PANX1 function in live cells (either pharmacologically or using the PANX1 DN mutant) did not cause apoptopodia (data not shown), suggesting that pannexin channels regulate the formation of these membrane protrusions after apoptosis induction. These apoptopodia were also observed in apoptotic thymocytes from PANX1 knockout mice, or wild-type thymocytes treated with pannexin inhibitors (Fig. 3j). Fas-, Dex- or UV-induced apoptosis led to apoptopodia formation when PANX1 function was impaired (data not shown).

We next asked how the apoptopodia formation and membrane blebbing were linked. PANX1-mediated TO-PRO-3 uptake began before the onset of blebbing (Fig. 4c), but the apoptopodia was detectable only after the onset of blebbing (Fig. 4b,g). This suggests that PANX1 activity is likely continuously required during apoptosis progression to downregulate the formation of apoptopodia. Interestingly, when blebbing was blocked by inhibiting actomyosin contraction or the Rho-dependent kinase ROCK (which are needed for apoptotic blebbing[22,30,31]), apoptopodia formation was unaffected, with noticeable absence of blebs at the end of these strings (Extended Data Fig. 8a-c). Importantly, inhibiting blebbing reduced the formation of apoptotic bodies in Jurkat cells with PANX1 function disrupted, pharmacological block, or in PANX1 deficient thymocytes (Extended Data Fig. 8d-f). These data suggest that the apoptopodia that arise due to PANX1 inhibition are independent of blebbing, but the annexin V[+] vesicular structures seen at the end of apoptopodia are dependent on blebbing and contribute to apoptotic bodies formation. LR73 fibroblasts induced to undergo apoptosis also showed the formation of apoptopodia and apoptotic bodies when PANX1 function was impaired (Extended Data Fig. 9). Thus, trovafloxacin-mediated enhancement of apoptotic bodies formation helped uncover a new step during early stages of apoptosis; specifically, pannexin channel function is required to restrain detachment of blebs from the apoptotic cells, and in turn, regulate the nature of apoptotic cell disassembly (Extended Data Fig. 10).

While quinolone antibiotics are effective in killing bacteria by targeting their topoisomerases, and are used worldwide to treat various bacteria infections[32-34], some quinolones have serious side effects (incidence up to 5%) in the liver, skin, tendon, gastrointestinal tract, central nervous system and cardiovascular system that are not readily explained[16,17]. Surprisingly, in contrast to trovafloxacin, two other structurally related quinolone antibiotics ciprofloxacin and levofloxacin did not block PANX1-dependent dye uptake, (Fig. 1c), despite all three being equally effective in inhibiting bacterial growth

(Extended Data Fig. 1j). Comparing the molecular structure of trovafloxacin with ciprofloxacin and levofloxacin suggested that certain features of trovafloxacin, such as the fluorinated ring at position N1 (Fig. 4h), might contribute to its effect on PANX1 (Fig. 1c and 2d). We next asked whether other quinolones with a fluorinated ring at position N1 can inhibit PANX1, and tested difloxacin and tosulfoxacin (Fig. 4h) that are currently available commercially in some Asian countries. Although less potent than trovafloxacin, both difloxacin and tosulfoxacin partially inhibited ATP release and TO-PRO-3 uptake by apoptotic cells, and promoted the formation of apoptotic bodies (Fig. 4i). These data do not exclude other molecular features of trovafloxacin that may also contribute to PANX1 inhibition, such as the C7 position of the quinolone (Fig. 4h).

The data presented here suggest an unexpected but intriguing link between the antibiotic trovafloxacin, eukaryotic pannexin channels, and a specific step in progression through apoptosis. Specifically, they provide three key insights. First, trovafloxacin, originally marketed by Pfizer showed tremendous promise, but was linked to severe toxicity and unexplained deaths among children in a trial in Nigeria, and was discontinued[16,35]. Since billions of cells are turned over daily via caspase-mediated apoptosis in the human body as part of normal life, and trovafloxacin can directly inhibit the mammalian PANX1 channels at doses normally achieved in humans, this could, in part, provide a mechanism for trovafloxacin toxicity.

Second, our data identify a new role for pannexin channels in maintaining cellular integrity during apoptosis. Fragmentation of apoptotic cells into smaller apoptotic bodies has been seen *in vitro* and *in vivo*[22], but the mechanism(s) regulating this disassembly process is not well understood. The trovafloxacin-mediated blockage of PANX1 uncovered a previously unappreciated step during apoptosis, and revealed an essential and non-redundant role for pannexin channels in the ordered disassembly of apoptotic cells.

Third, the dearth of new antibiotics in the pipeline despite the steady increase in drug-resistant bacteria worldwide[33,34] is a significant health threat[36]. Interestingly, quinolone antibiotics such as ciprofloxacin and levofloxacin do not share the inhibitory effect of trovafloxacin towards the mammalian PANX1, and certain features in trovafloxacin might in part explain its toxicity. Further studies on the interaction of quinolones with PANX1 and the associated apoptosis pathways may provide clues to the underlying reasons for the idiosyncratic and irreversible liver toxicity observed with trovafloxacin. Unlocking such clues could re-invigorate industrial interest in the quinolone class for the production of safer, and more potent antibacterials.

Online-Only Methods

Reagents

Library of Pharmacologically Active Compounds (LOPAC[1280TM]), trovafloxacin, ciprofloxacin, levofloxacin, difloxacin, tosufloxacin, carbenoxolone, probenecid, Y-27632, blebbistatin, cytochalasin D, purified nucleotides, suramin and dexamethasone were obtained from Sigma-Aldrich. 7-AAD and TO-PRO-3 were purchased from Invitrogen. annexin V-FITC, CD8a-PE (clone 53-6.7), CD4-PE-Cy7 (clone RM4-5) and anti-mouse

CD16/CD32 (clone 93) were obtained for eBioscience. Other reagents were obtained as follows: anti-Fas (clone CH11, Millipore), z-VAD-FMK (Enzo Life Sciences), Q-VD-OPH (SM Biochemicals) and recombinant apyrase (New England Biolabs).

Induction of apoptosis

Jurkat cells in RPMI/1% BSA were treated with 250 ng ml^{-1} anti-Fas (clone CH11) or 150 mJ cm^{-2} ultraviolet C irradiation (Stratalinker). Primary thymocytes (collected from 5 to 7-week-old C57BL/6 mice, male and female) were treated with 50 μM dexamethasone for 5h. LR73 cells were treated with 150 mJ cm^{-2} ultraviolet C irradiation for 6h. All treatments were incubated for indicated times at 37°C, 5% CO_2, unless noted otherwise.

Drug screening for regulators of PANX1 function

Jurkat cells (1×10^6 cells ml^{-1} in DMEM/0.5% BSA) were induced to undergo apoptosis by anti-Fas treatment (250 ng ml^{-1}) in the presence of 10 μM of compounds in the LOPAC^{1280TM} (Sigma-Aldrich) for 4h at 37°C, 5% CO_2. Cells were then stained with TO-PRO-3 (0.67 μM) for 10 min at room temperature and immediately placed on ice prior to analysis on a BD FACSCanto flow cytometer. The resultant flow cytometric data were analyzed by FlowJo software (Tree Star).

Determining cell viability by flow cytometry and ImageStream

Samples were stained with annexin V-FITC, 7-AAD and TO-PRO-3 in annexin V binding buffer for 10 min at room temperature and immediately placed on ice prior to analysis on a BD FACSCanto flow cytometer, with the resultant flow cytometry data analyzed by FlowJo software. Samples were also prepared the same way prior to analysis on an ImageStreamX Mark II (Amnis), with the resultant data analyzed by IDEAS software (Amnis).

For TO-PRO-3 uptake assay following acute drug treatment, Jurkat cells in RPMI/1% BSA were treated with 500 ng ml^{-1} anti-Fas (clone CH11) for 4h at 37°C, 5% CO_2. Following induction of apoptosis, cells were treated with pan caspase inhibitor Q-VD-OPH (50 μM) and the indicated concentrations of compounds for 20 min at 37°C, 5% CO_2. Cells were subsequently stained with annexin V-FITC, 7-AAD and TO-PRO-3 and analyzed on a FACSCanto flow cytometer. The resultant flow cytometry data were analyzed by FlowJo software (Tree Star).

Generation of pannexin 1 knockout mice

Panx1 targeted ES cells (EPD0309-3-B01) were obtained from the Knockout Mouse Project (KOMP) Repository. After blastocyst injections (performed by the transgenic core facility at the University of Virginia), chimaeras were bred with C57BL/6J mice (JaxMice). The resultant offspring were crossed with β-actin/Flp mice (JaxMice) to delete the neomycin cassette, thereby generating mice carrying a floxed *Panx1* exon 3 allele (*Panx1$^{fl/fl}$*) (Extended Data Fig. 7). To generate *Panx1* global knockout mice, *Panx1$^{fl/fl}$* mice were crossed with *EIIa*-Cre mice (JaxMice) expressing Cre from the two-cell stage of embryonic development to delete *Panx1* exon 3 in all tissues[37]. Resulting mice were crossed with C57BL/6J mice to remove Flp and Cre from the background. To generate mice that carry deletion of *Panx1* specifically in thymocytes, *Panx1$^{fl/fl}$* mice were crossed with *Lck*-Cre

mice (JaxMice) expressing Cre under the *Lck* proximal promoter, which mediates deletion of *Panx1* exon 3 from the double-negative stage of thymocyte development[38].

Microscopy

Live imaging was performed on a Zeiss microscope using a 40x or 60x oil immersion objective in a 37°C/5% CO_2 atmosphere. Jurkat cells at 5×10^5 cells ml^{-1} in RPMI/1% BSA (600 μl) were seeded onto Lab-Tek II Chambered Coverglass (Nunc) by two successive centrifugations at 20*g* for 1 min prior to imaging. LR73 fibroblasts were cultured overnight on Chambered Coverglass prior to imaging. In certain experiments, TO-PRO-3 and annexin V-FITC were also present during the imaging process.

Bacterial growth assay

Overnight *Escherichia coli* culture was diluted 100 fold in LB medium prior to incubation with quinolones for 6h. Bacterial growth was monitored by the absorbance at 600 nm using a FlexStation 3 plate reader, with the resultant data analyzed using SoftMaxPro 5.4 software.

Nucleotide measurement

ATP in apoptotic cell supernatants was measured using a luciferase/luciferin assay (CellTiter-Glo; Promega) according to manufacturer's instructions.

Caspase activation

Caspase 3/7 activity assayswere performed with the Caspase-Glo 3/7 (Promega) reagents, in accordance with the manufacturer's instructions.

Immunoblotting

Samples were analyzed by SDS-PAGE and immunoblotting using the following dilutions: anti-GFP (1:1,000; Santa Cruz), anti-ERK2 (1:3,000; Santa Cruz), anti-Caspase 3 (1:2,500; Santa Cruz) and affinity purified rabbit anti-mouse PANX1 (0.2 μg ml^{-1}).

Patch-clamp analysis

Electrophysiological recordings were made at room temperature using an Axopatch 200B amplifier (Molecular Devices). Whole-cell recordings were carried out in Jurkat cells or transiently transfected HEK293T cells with borosilicate glass patch pipettes (3-5 MΩ). Bath solution contained 140 mM NaCl, 3 mM KCl, 2 mM $MgCl_2$, 2 mM $CaCl_2$, 10 mM HEPES, and 10 mM glucose (pH 7.3). Pipette solution was composed of 30 mM tetraethylammonium chloride, 100 mM $CsMeSO_4$, 4 mM NaCl, 1 mM $MgCl_2$, 0.5 mM $CaCl_2$, 10 mM HEPES, 10 mM EGTA, 3 mM ATP-Mg, and 0.3 mM GTP-Tris (pH 7.3). A ramp voltage command was applied using pCLAMP software and a Digidata 1322A digitizer (Molecular Devices). Data were analyzed using pCLAMP software. Results were presented as means ± s.e.m. The dose-response curve was fitted and IC50 was determined using Prism 5 software. Inside-out patch recordings were obtained using patch pipettes (2-4 MΩ) filled with the bath solution (described above) in a perfusate containing 150 mM CsCl, 5 mM EGTA, 1 mM MgCl2,, 10 mM HEPES (pH 7.3). Currents were evoked from a

holding potential of -50 mV. All-point histograms and NPo analysis was performed using pCLAMP software. Cx43 currents were measured in divalent-free bath solution[39].

DNA fragmentation assay

DNA laddering during apoptosis was characterized by agarose gel electrophoresis [40]. In brief, 60,000 Jurkat cells were induced to undergo apoptosis by anti-Fas treatment for 2h and lysed in TES lysis buffer containing RNase for 2h at 37°C. Cell lysates were subsequently treated with proteinase K for 18h at 50°C and DNA fragmentation was visualized by agarose gel electrophoresis.

Quantitative PCR

cDNA was synthesized from 50 ng of RNA isolated from primary thymocytes (RNeasy, Qiagen) using Superscript III (Invitrogen). Quantitative PCR was performed on the ABI StepOnePlus Real-time PCR instrument with TaqMan probes (Applied Biosystems). Levels of mouse *Panx1* mRNA are normalized to *gapdh*. TaqMan probes used were: mouse *Panx1* (Mm00450900_m1) and mouse *gapdh* (4352339E-1207039).

In vivo model of apoptosis

5-week-old C57BL/6 mice (male and female) were injected intraperitoneally with 12.5 mg/kg dexamethasone. Thymocytes were collected 6h post dexamethasone injection, stained with annexin V-FITC, 7-AAD, TO-PRO-3, CD8a-PE and CD4-PE-Cy7, and analyzed on a BD FACSCanto flow cytometer. The University of Virginia Animal Care and Use Committee approved all animal experiments.

Statistical analyses

Data are presented as means ± s.e.m. Statistical significance for comparisons was determined by unpaired Student's two-tailed *t*-test. A P value less than 0.05 was considered statistically significant. * $P < 0.05$, ** $P < 0.01$, *** $P < 0.001$.

Supplementary Material

Refer to Web version on PubMed Central for supplementary material.

Acknowledgments

References

1. Penuela S, Gehi R, Laird DW. The biochemistry and function of pannexin channels. Biochim Biophys Acta. 2013; 1828:15–22. [PubMed: 22305965]

2. Sosinsky GE, et al. Pannexin channels are not gap junction hemichannels. Channels (Austin). 2011; 5:193–197. [PubMed: 21532340]

3. Chen Y, et al. Purinergic signaling: a fundamental mechanism in neutrophil activation. Sci Signal. 2010; 3:ra45. [PubMed: 20530802]

4. Seminario-Vidal L, et al. Rho signaling regulates pannexin 1-mediated ATP release from airway epithelia. The Journal of biological chemistry. 2011; 286:26277–26286. [PubMed: 21606493]

5. Seror C, et al. Extracellular ATP acts on P2Y2 purinergic receptors to facilitate HIV-1 infection. J Exp Med. 2011; 208:1823–1834. [PubMed: 21859844]

6. Billaud M, Sandilos JK, Isakson BE. Pannexin 1 in the regulation of vascular tone. Trends Cardiovasc Med. 2012; 22:68–72. [PubMed: 22841835]

7. Karatas H, et al. Spreading depression triggers headache by activating neuronal Panx1 channels. Science. 2013; 339:1092–1095. [PubMed: 23449592]

8. Kim JE, Kang TC. The P2X7 receptor-pannexin-1 complex decreases muscarinic acetylcholine receptor-mediated seizure susceptibility in mice. The Journal of clinical investigation. 2011; 121:2037–2047. [PubMed: 21505260]

9. MacVicar BA, Thompson RJ. Non-junction functions of pannexin-1 channels. Trends in neurosciences. 2010; 33:93–102. [PubMed: 20022389]

10. Lazarowski ER. Vesicular and conductive mechanisms of nucleotide release. Purinergic Signal. 2012; 8:359–373. [PubMed: 22528679]

11. Dubyak GR. Ion homeostasis, channels, and transporters: an update on cellular mechanisms. Advances in physiology education. 2004; 28:143–154. [PubMed: 15545343]

12. Elliott MR, et al. Nucleotides released by apoptotic cells act as a find-me signal to promote phagocytic clearance. Nature. 2009; 461:282–286. [PubMed: 19741708]

13. Chekeni FB, et al. Pannexin 1 channels mediate 'find-me' signal release and membrane permeability during apoptosis. Nature. 2010; 467:863–867. [PubMed: 20944749]

14. Sandilos JK, et al. Pannexin 1, an ATP release channel, is activated by caspase cleavage of its pore-associated C-terminal autoinhibitory region. The Journal of biological chemistry. 2012; 287:11303–11311. [PubMed: 22311983]

15. Qu Y, et al. Pannexin-1 is required for ATP release during apoptosis but not for inflammasome activation. J Immunol. 2011; 186:6553–6561. [PubMed: 21508259]

16. Liu HH. Safety profile of the fluoroquinolones: focus on levofloxacin. Drug safety : an international journal of medical toxicology and drug experience. 2010; 33:353–369.

17. Stahlmann R, Lode H. Safety considerations of fluoroquinolones in the elderly: an update. Drugs & aging. 2010; 27:193–209. [PubMed: 20210367]

18. Bruzzone R, Barbe MT, Jakob NJ, Monyer H. Pharmacological properties of homomeric and heteromeric pannexin hemichannels expressed in Xenopus oocytes. J Neurochem. 2005; 92:1033–1043. [PubMed: 15715654]

19. Ma W, Hui H, Pelegrin P, Surprenant A. Pharmacological characterization of pannexin-1 currents expressed in mammalian cells. J Pharmacol Exp Ther. 2009; 328:409–418. [PubMed: 19023039]

20. Vincent J, et al. Pharmacokinetics and safety of trovafloxacin in healthy male volunteers following administration of single intravenous doses of the prodrug, alatrofloxacin. The Journal of antimicrobial chemotherapy. 1997; 39 Suppl B:75–80. [PubMed: 9222074]

21. Teng R, Liston TE, Harris SC. Multiple-dose pharmacokinetics and safety of trovafloxacin in healthy volunteers. The Journal of antimicrobial chemotherapy. 1996; 37:955–963. [PubMed: 8737145]

22. Wickman G, Julian L, Olson MF. How apoptotic cells aid in the removal of their own cold dead bodies. Cell Death Differ. 2012; 19:735–742. [PubMed: 22421963]

23. Moss DK, Betin VM, Malesinski SD, Lane JD. A novel role for microtubules in apoptotic chromatin dynamics and cellular fragmentation. J Cell Sci. 2006; 119:2362–2374. [PubMed: 16723742]

24. Nagata S, Hanayama R, Kawane K. Autoimmunity and the clearance of dead cells. Cell. 2010; 140:619–630. [PubMed: 20211132]

25. Bortner CD, Cidlowski JA. Caspase independent/dependent regulation of K(+), cell shrinkage, and mitochondrial membrane potential during lymphocyte apoptosis. J Biol Chem. 1999; 274:21953–21962. [PubMed: 10419518]

26. Vanden Berghe T, et al. Determination of apoptotic and necrotic cell death in vitro and in vivo. Methods. 2013; 61:117–129. [PubMed: 23473780]

27. Silverman W, Locovei S, Dahl G. Probenecid, a gout remedy, inhibits pannexin 1 channels. Am J Physiol Cell Physiol. 2008; 295:C761–767. [PubMed: 18596212]

28. Cohen JJ, Duke RC, Fadok VA, Sellins KS. Apoptosis and programmed cell death in immunity. Annu Rev Immunol. 1992; 10:267–293. [PubMed: 1590988]

29. Baroja-Mazo A, Barbera-Cremades M, Pelegrin P. The participation of plasma membrane hemichannels to purinergic signaling. Biochim Biophys Acta. 2013; 1828:79–93. [PubMed: 22266266]

30. Coleman ML, et al. Membrane blebbing during apoptosis results from caspase-mediated activation of ROCK I. Nat Cell Biol. 2001; 3:339–345. [PubMed: 11283606]

31. Sebbagh M, et al. Caspase-3-mediated cleavage of ROCK I induces MLC phosphorylation and apoptotic membrane blebbing. Nat Cell Biol. 2001; 3:346–352. [PubMed: 11283607]

32. Andriole VT. The quinolones: past, present, and future. Clin Infect Dis. 2005; 41 Suppl 2:S113–119. [PubMed: 15942877]

33. Antibiotic resistance threats in the United States, 2013: Report by Centers for Disease Control and Prevention - US Department of Health and Human Services. 2013

34. UK Five Year Antimicrobial Resistance Strategy 2013 to 2018: Report by the Department of Health, United Kingdom. 2013

35. Ahmad K. Drug company sued over research trial in Nigeria. Lancet. 2001; 358:815. [PubMed: 11564494]

36. Spellberg B, et al. The epidemic of antibiotic-resistant infections: a call to action for the medical community from the Infectious Diseases Society of America. Clin Infect Dis. 2008; 46:155–164. [PubMed: 18171244]

37. Lakso M, et al. Efficient in vivo manipulation of mouse genomic sequences at the zygote stage. Proc Natl Acad Sci U S A. 1996; 93:5860–5865. [PubMed: 8650183]

38. Lee PP, et al. A critical role for Dnmt1 and DNA methylation in T cell development, function, and survival. Immunity. 2001; 15:763–774. [PubMed: 11728338]

39. Harris AL. Connexin channel permeability to cytoplasmic molecules. Prog Biophys Mol Biol. 2007; 94:120–143. [PubMed: 17470375]

40. Henry CM, Hollville E, Martin SJ. Measuring apoptosis by microscopy and flow cytometry. Methods. 2013; 61:90–97. [PubMed: 23403105]
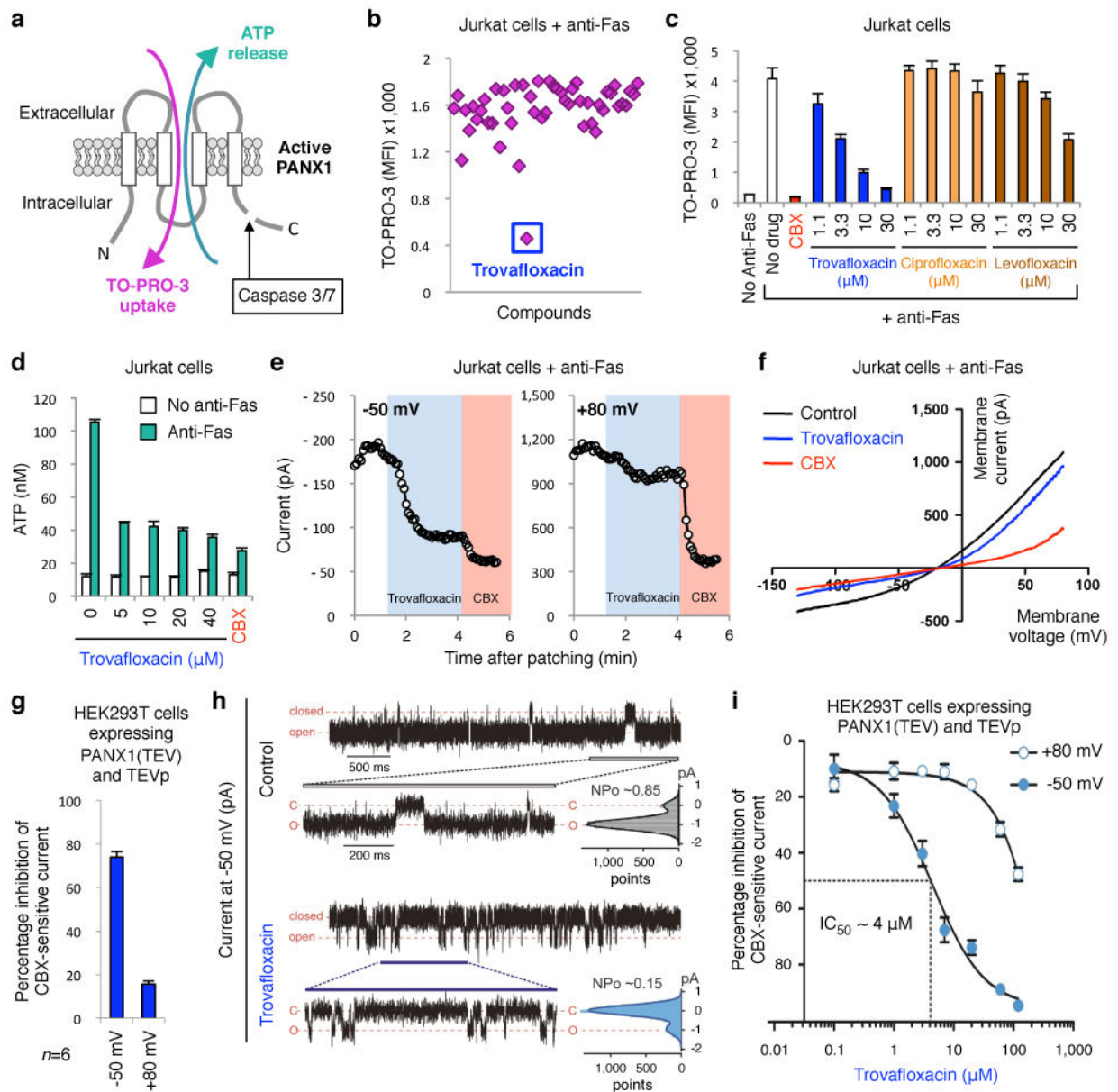
Figure 1. Trovafloxacin inhibits pannexin 1 activity during apoptosis
a, Schematic of PANX1 with ATP release and TO-PRO-3 uptake by apoptotic cells after caspase-mediated channel opening. **b**, Subset of LOPAC^{1280TM} library screen in modulating TO-PRO-3 uptake (MFI average of 1200-1800), with inhibition by trovafloxacin indicated. **c**, Dose-dependent inhibition of TO-PRO-3 uptake by trovafloxacin (or positive control CBX), levofloxacin and ciprofloxacin (n=3). **d**, Inhibition of ATP release from apoptotic cells by trovafloxacin (n=3). **e**, Patch-clamp recordings from apoptotic cells at -50mV and +80mV with trovafloxacin (blue shading) or CBX (pink); traces are representative of recordings from 7 cells per group. **f**, Current-voltage relationships (I-V curves) from apoptotic cells over a range of voltages (n=7). **g**, Trovafloxacin inhibition of CBX-sensitive current in HEK293T cells expressing TEV-protease activated PANX1 channels (n=6). **h**,

Inside-out patch clamp recordings from excised patches containing TEV-cleaved PANX1 channels showing traces of inward currents at -50mV. PANX1 channels are mostly 'open' without trovafloxacin (open probability, NPo=0.85), while mostly closed with trovafloxacin (NPo=0.15); histograms of channel activity are shown for each trace (n=3). **i**, Inhibition of TEV-cleaved open PANX1 channels by trovafloxacin, with IC_{50} of 4μM at -50mV (n 6 per data point). **e**,**f**, Jurkat cells after 2h with anti-Fas used for patch-clamp recordings. Error bars represent s.e.m.
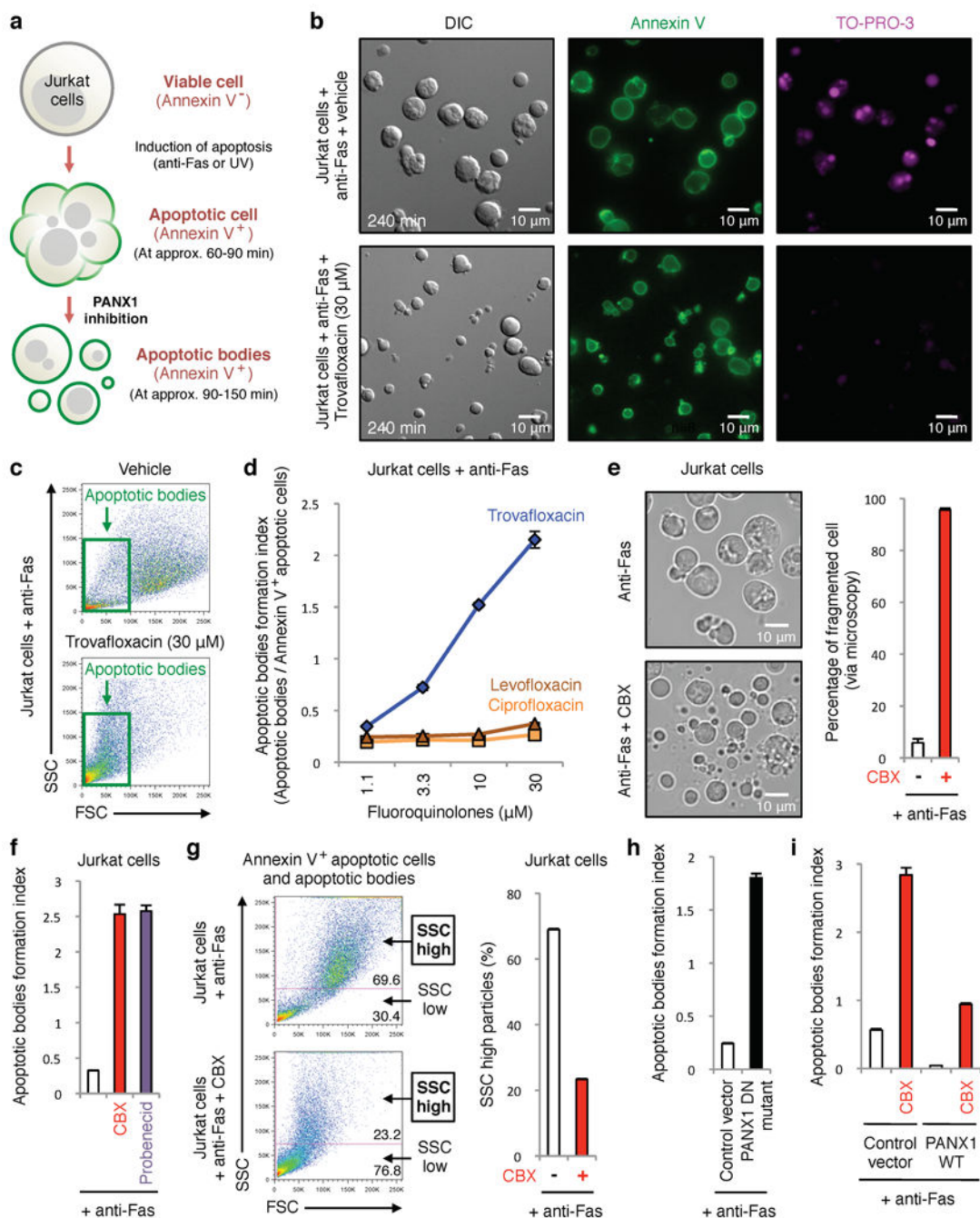
Figure 2. Trovafloxacin-mediated inhibition of PANX1 promotes formation of smaller apoptotic bodies

a, Schematic for apoptosis progression and generation of apoptotic bodies, derived from multi-parameter time-lapse analyses of Jurkat cells. **b**, Images of vehicle- or trovafloxacin-treated apoptotic cells stained with annexin V or TO-PRO-3. Note the annexin V[positive], TO-PRO-3[negative] apoptotic bodies (∼0.9-5μm) after trovafloxacin treatment. **c**, Trovafloxacin increases particles with reduced size (FSC) and complexity (SSC). **d**, Generation of apoptotic bodies is enhanced by trovafloxacin, but not levofloxacin and ciprofloxacin (*n*=3).

e, Left, representative 4h time-lapse images monitoring apoptotic cell morphology (454 cells for untreated and 355 cells for CBX-treated, *n*=3). Right, percentage of cell fragmentation (2 fragments). **f**, Apoptotic bodies formation index (apoptotic bodies/annexin V$^+$ apoptotic cells) is enhanced by PANX1 blockers CBX or probenecid (*n*=3). **g**, Left, Size (FSC) and complexity (SSC) of particles from apoptotic cells with or without CBX. Right, percentage of SSC^{high} particles. **h,i**, Formation of apoptotic bodies is increased in Jurkat cells expressing PANX1 DN mutant, but decreased in PANX1 WT transfected cells (*n*=3). The PANX1 WT effect is reversed by CBX. Error bars represent s.e.m. Scale bars represent 10μm.
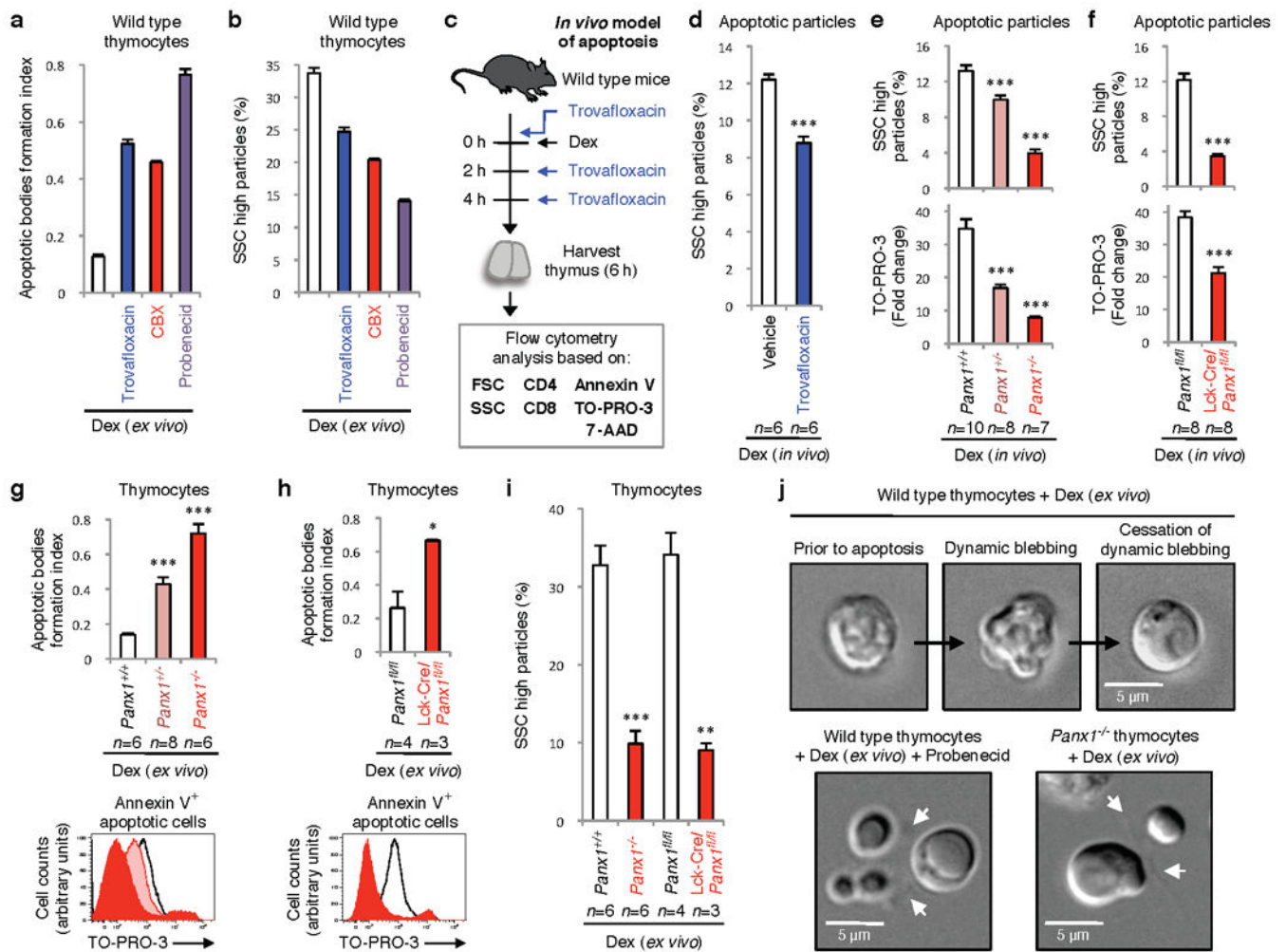
Figure 3. Pannexin 1 regulates disassembly of apoptotic thymocytes

Increase in formation of apoptotic bodies (**a**), or decreases SSC^{high} particles (**b**) from dexamethasone (dex)-treated thymocytes *ex vivo* by trovafloxacin, CBX, and probenecid (*n*=3). **c**, Schematic for testing trovafloxacin in thymic apoptosis *in vivo*. **d**, Reduction in SSC^{high} apoptotic bodies in thymi of wild-type mice treated with dex+trovafloxacin (*n*=6). **e,f**, Complexity and TO-PRO-3 uptake (fold change relative to unstained) in thymi of indicated mice injected intraperitoneally with dex (*n*=10 for *Panx1$^{+/+}$*, *n*=8 for *Panx1$^{+/-}$*, *n*=7 for *Panx1$^{-/-}$*, *n*=8 for *Panx1$^{fl/fl}$* and Lck-Cre/*Panx1$^{fl/fl}$*). **g,h**, Formation of apoptotic bodies (upper) or TO-PRO-3 uptake (lower) in *ex vivo* in dex-treated thymocytes from *Panx1$^{-/-}$* or Lck-Cre/*Panx1$^{fl/fl}$* thymocytes. **i**, Reduction in SSC^{high} subcellular apoptotic particles in thymocytes from *Panx1$^{-/-}$* and Lck-Cre/*Panx1$^{fl/fl}$* mice. (**g,h,i**, *n*=6 for *Panx1$^{+/+}$*, *n*=8 for *Panx1$^{+/-}$*, *n*=6 for *Panx1$^{-/-}$*, *n*=4 for *Panx1$^{fl/fl}$*, *n*=3 for Lck-Cre/*Panx1$^{fl/fl}$*). **j**, Time-lapse images monitoring apoptotic cell morphology of thymocytes. Arrows, apoptopodia. Error bars represent s.e.m. Scale bars=5μm. Data in **a**, **b** and **j** are representative of at least two independent experiments. See Extended Data Fig. 5 and 6 for gating strategy. * $P < 0.05$, ** $P < 0.01$, *** $P < 0.001$, unpaired Student's two-tailed *t*-test.
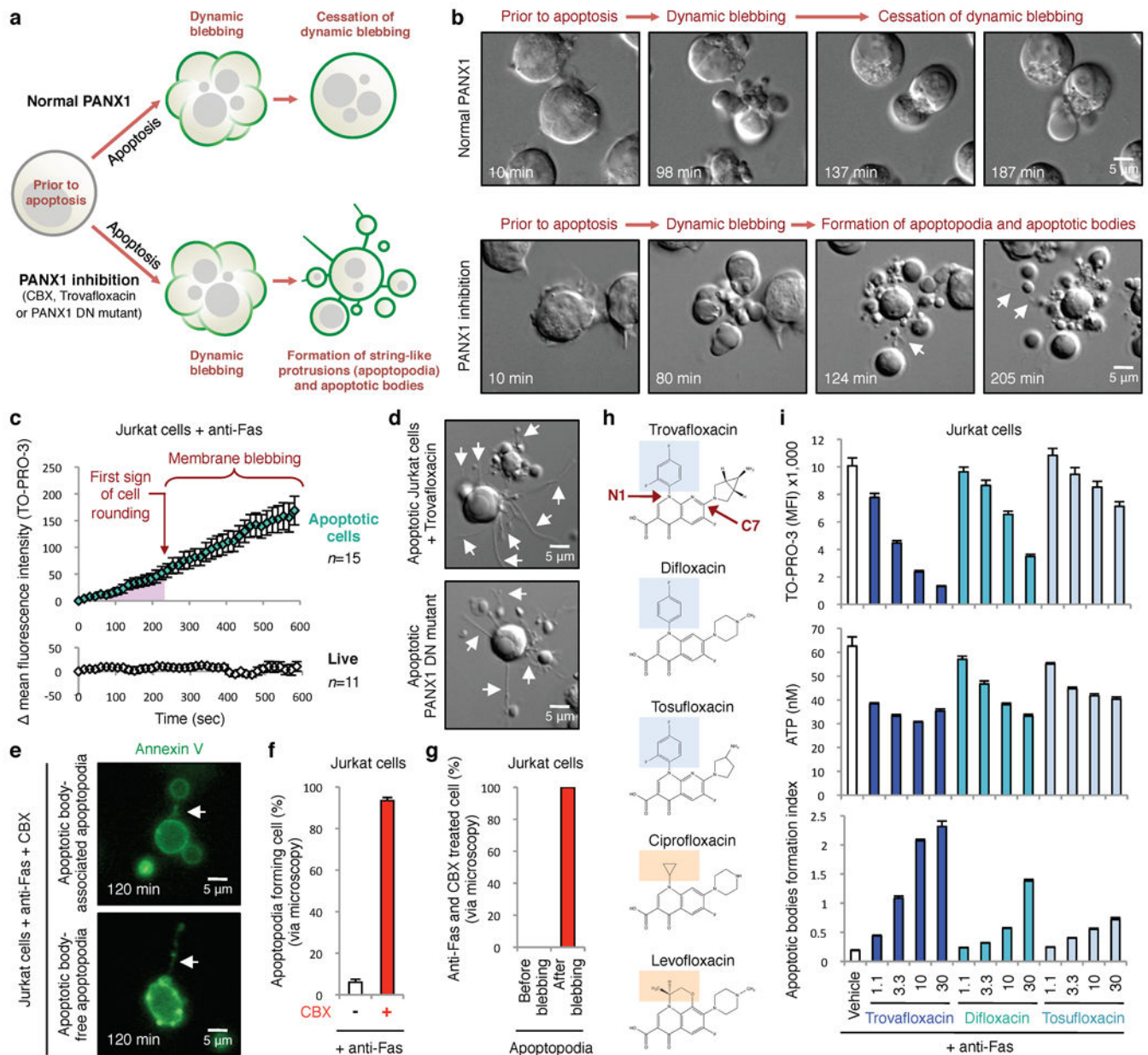
Figure 4. Formation of string-like apoptopodia after membrane blebbing correlates with formation of apoptotic bodies

a, Schematic of apoptotic Jurkat cells with normal or impaired PANX1, based on time-lapse microscopy. **b**, Time-lapse images monitoring progression of apoptotic cell morphology. **c**, PANX1-mediated TO-PRO-3 entry occurs prior to membrane blebbing as determined by quantitating TO-PRO-3 uptake by apoptotic cells (n=15) in time-lapse imaging (normalized to first sign of cell rounding). TO-PRO-3 uptake was undetectable in live cells (n=11). **d**, Trovafloxacin-treated apoptotic cells or expressing PANX1-DN mutant show formation of apoptopodia. **e**, Apoptopodia have membranes with exposed phosphatidylserine and apoptotic blebs at the end of the protrusion. **f**, Percentage of apoptotic cells with apoptopodia during 4h of time-lapse imaging. **g**, Apoptopodia are barely detectable before

onset of membrane blebbing in cells with impaired PANX1 function, but detected after initiation of blebbing. (**f,g**, 429 and 302 cells for untreated and CBX-treated, respectively, *n*=3). **h**, Chemical structures of quinolones used, with the N1 fluorinated ring (blue) indicated in quinolones that inhibit PANX1 (trovafloxacin, difloxacin, and tosufloxacin), compared to quinolones with no apparent PANX1 inhibition (ciprofloxacin and levofloxacin) orange. **i**, TO-PRO-3 uptake, ATP release, and formation of apoptotic bodies from apoptotic Jurkat cells treated with trovafloxacin, difloxacin or tosufloxacin (*n*=3). Error bars represent s.e.m. Scale bars represent 5μm. Arrows, apoptopodia. Data are representative of at least two independent experiments.
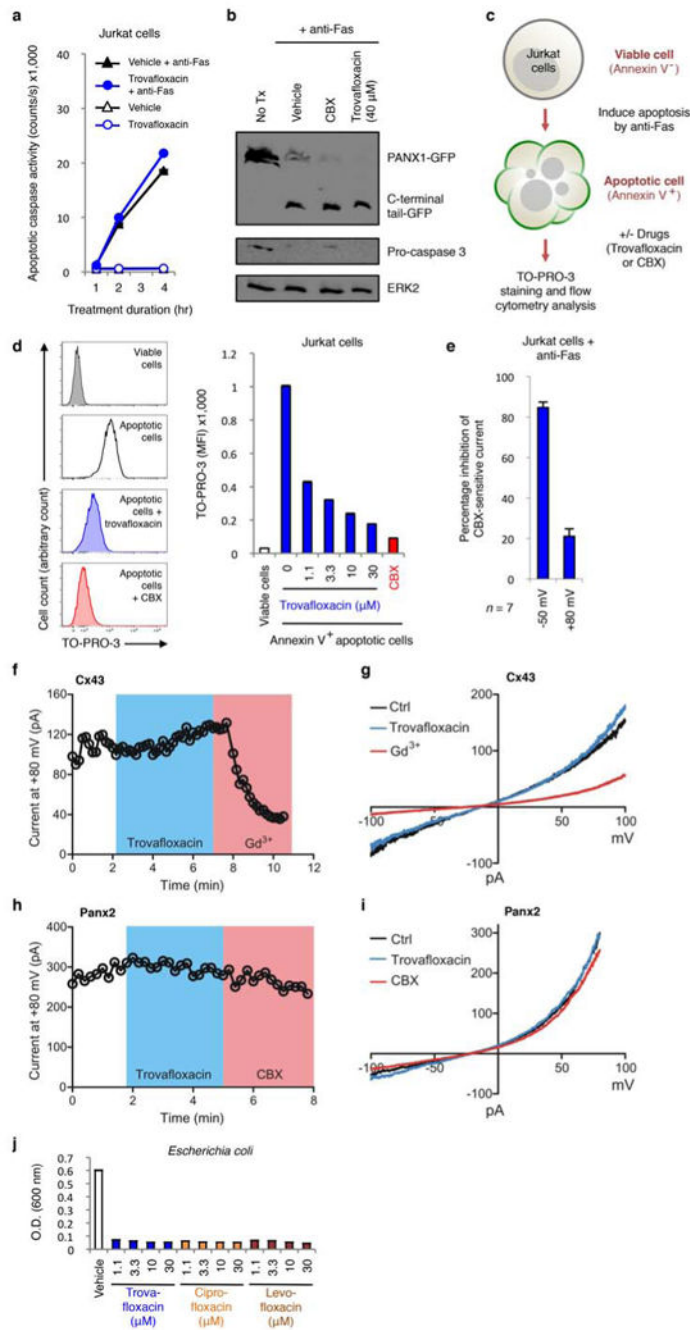
Extended Data Figure 1. Trovafloxacin does not block caspase activation or inhibit connexin 43 (Cx43) or pannexin 2 (Panx2) membrane currents

a, Caspase 3/7 activation in Jurkat cells undergoing apoptosis is not altered by treatment with trovafloxacin (40 μM) (*n*=3). **b**, Proteolytic cleavage of PANX1-GFP during apoptosis is not inhibited by trovafloxacin (40 μM) or CBX (500 μM) treatment. **c**, Schematic diagram for the acute treatment of apoptotic cells with trovafloxacin or CBX. **d**, Acute trovafloxacin treatment inhibits TO-PRO-3 uptake by apoptotic Jurkat cells. Left, histograms showing TO-PRO-3 uptake by viable cells, apoptotic cells, or apoptotic cells treated with

trovafloxacin or CBX (500 μM) post induction of apoptosis and analyzed by flow cytometry. Right, uptake of TO-PRO-3 presented as (median fluorescence intensity, MFI) of viable cells or apoptotic cells (*n*=3). **e**, Inhibition of CBX-sensitive current in apoptotic cells treated with trovafloxacin (20 μM), as measured by whole-cell patch-clamp recording (*n*=7). **f**, Patch-clamp recordings from HEK293T cells expressing the Cx43 and receiving indicated treatments. Whole-cell current at +80 mV is shown under conditions when bath solution was perfused with trovafloxacin (20 μM, blue shading) or gadolinium (Gd^{3+}) (100 μM, pink shading). Exemplar traces are representative of 14 cells per group. **g**, Current-voltage relationships of Cx43 current in HEK293T cells treated with or without trovafloxacin (20 μM) or Gd^{3+} (100 μM), with the current measured over a range of voltages. **h**, Patch-clamp recordings from HEK293T cells expressing the mouse Panx2 and receiving indicated treatments. Whole-cell current at +80 mV is shown under conditions when bath solution was perfused with trovafloxacin (20 μM, blue shading) or carbenoxolone (CBX) (50 μM, pink shading). Exemplar traces are representative of 4 cells per group. **i**, Current-voltage relationships of Panx2 current in HEK293T cells treat with or without trovafloxacin (20 μM) or CBX (50 μM), with the current measured over a range of voltages. **j**, Trovafloxacin, ciprofloxacin and levofloxacin inhibit bacterial growth. *Escherichia coli* growth (as measured by O.D. at 600 nm) in the presence of indicated concentrations of quinolones (*n*=3). Error bars represent s.e.m.
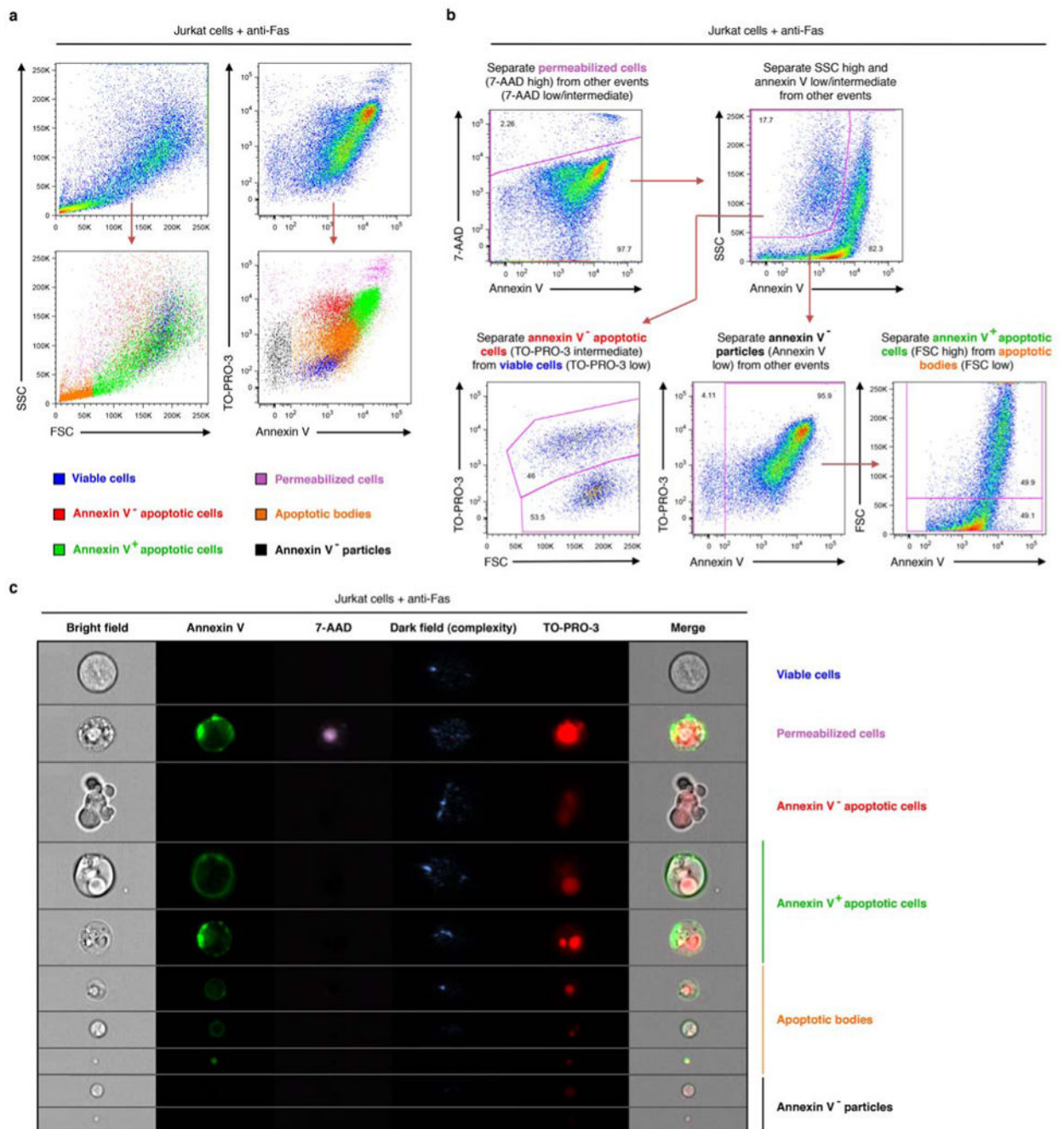
Extended Data Figure 2. Electronic gating strategy for the separation of different cellular and subcellular population of Jurkat cells undergoing apoptosis *in vitro*

a, Flow cytometric analysis showing each type of particles gated (see **b** below) has a distinctive level of cellular complexity (side scatter, SSC), cell size (forward scatter, FSC) as well as TO-PRO-3 (indicative of caspase-mediated activation of pannexin 1 channels), 7-AAD (indicative of membrane integrity) and annexin V (indicative of phosphatidylserine exposure) staining. **b**, Flow cytometry gating strategy used to distinguish viable cells, annexin V- apoptotic cells, annexin V+ apoptotic cells, annexin V- particles, and apoptotic

bodies. **c**, ImageStream analysis of particles gated using the same strategy as described in **b**. Representative images for each type of particles are shown. Jurkat cells were induced to undergo apoptosis by anti-Fas treatment (2 h) in all indicated experiments.
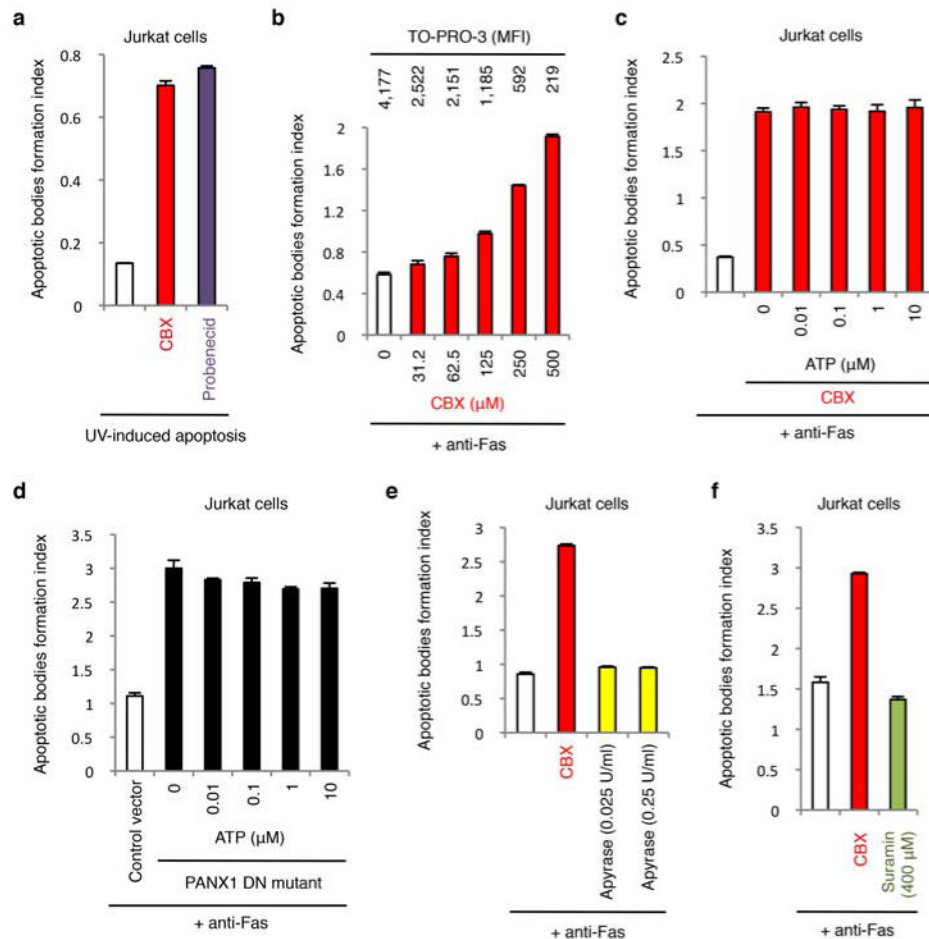
Extended Data Figure 3. Inhibition of pannexin 1 promotes the formation of apoptotic bodies via a mechanism independent of extracellular ATP

a, CBX and probenecid enhance the generation of apoptotic bodies from cells undergoing UV-induced apoptosis (n=3). **b**, Formation of apoptotic bodies after treatment with the indicated concentrations of CBX (n=3). The corresponding TO-PRO-3 uptake by annexin V^+ apoptotic cells at each CBX concentration is shown above the respective bars. **c,d**, Addition of exogenous ATP during apoptosis induction does not inhibit formation of apoptotic bodies in CBX-treated cells (n=3) (**c**) or cells stably expressing the dominant-negative PANX1 mutant (PANX1 DN mutant) (n=3) (**d**). **e**, Removal of extracellular ATP by apyrase does not promote formation of apoptotic bodies (n=3). **f**, P2Y receptor antagonist suramin does not promote formation of apoptotic bodies (n=3). Jurkat cells were induced to undergo apoptosis by anti-Fas treatment in all indicated experiments. Error bars represent s.e.m.
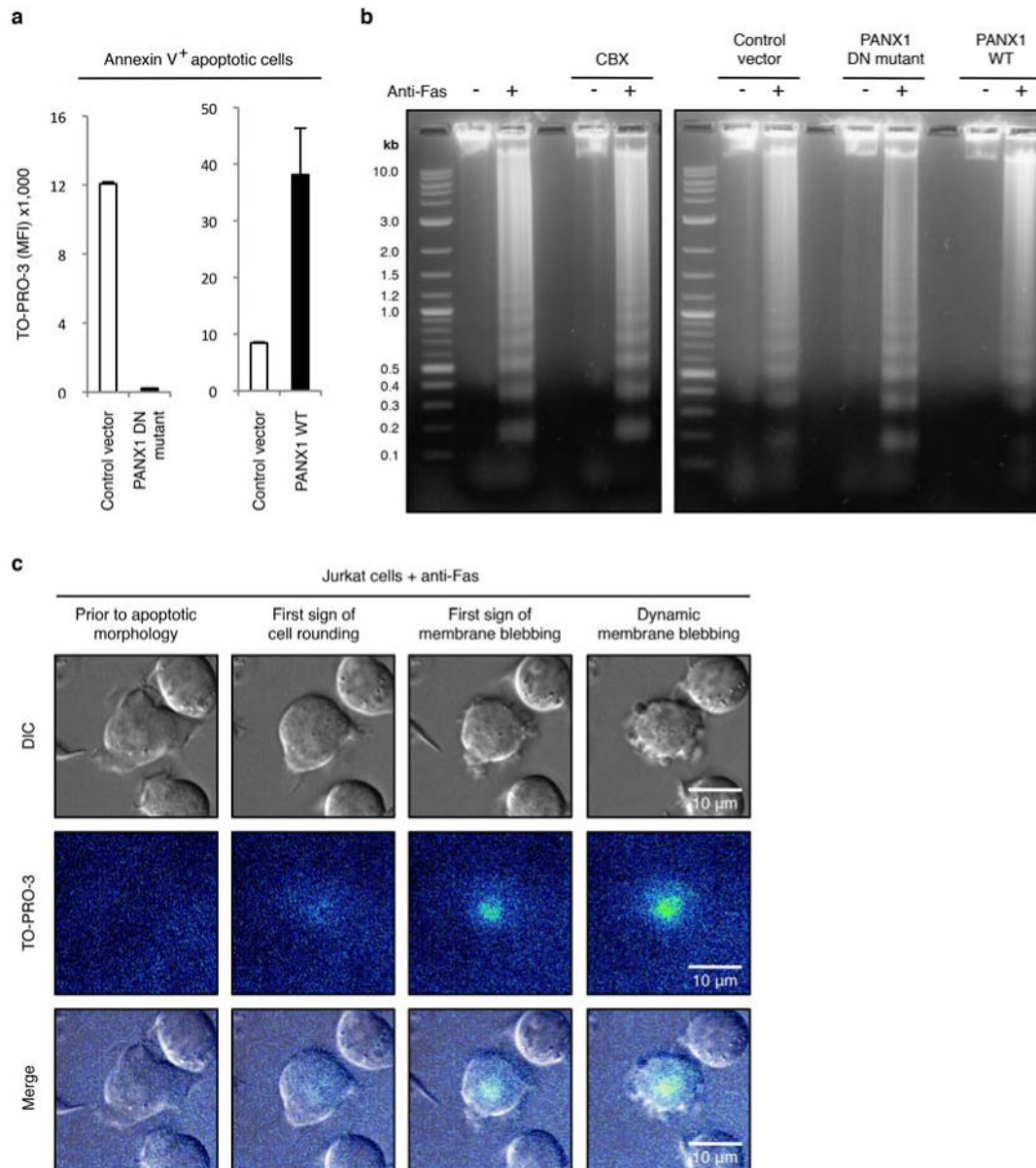
Extended Data Figure 4. Pannexin 1 activity does not affect DNA fragmentation during apoptosis

a,**b**, TO-PRO-3 dye uptake (*n*=3) (**a**) and DNA fragmentation (**b**) were assessed in Jurkat cells stably expressing the control vector, the dominant-negative PANX1 mutant (PANX1 DN mutant) or wild-type PANX1 (PANX1 WT). DNA fragmentation from cells induced to undergo apoptosis and treated with or without 500 μM CBX is also shown in **b. c**, Time-lapse images monitoring TO-PRO-3 dye uptake during progression of apoptosis in Jurkat cells with normal PANX1 function show that TO-PRO-3 uptake occurs prior to initiation of membrane blebbing. Jurkat cells were induced to undergo apoptosis by anti-Fas treatment (2 h). Error bars in **a** represent s.e.m.
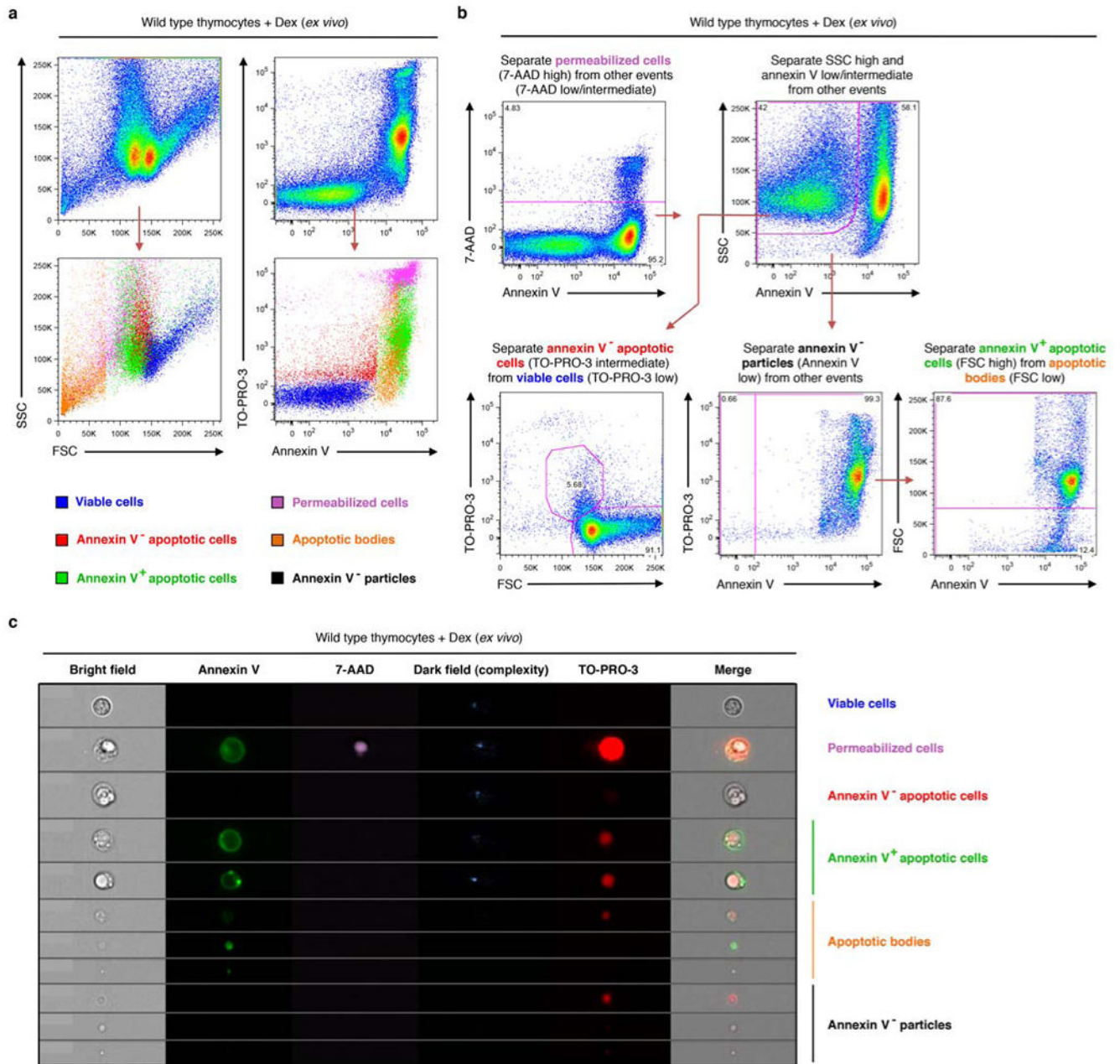
Extended Data Figure 5. Electronic gating strategy for the separation of different cellular and subcellular populations of primary thymocytes undergoing apoptosis *ex vivo*

a, Flow cytometry analysis showing each type of particles gated according to **b** has a distinctive level of SSC, FSC as well as TO-PRO-3 and annexin V staining. **b**, Flow cytometry analysis showing electronic gating strategy used to distinguish viable cells, annexin V- apoptotic cells, annexin V^+ apoptotic cells, annexin V^- particles, and apoptotic bodies. **c**, ImageStream analysis of particles gated using the same strategy as described in **b**. Representative images for each type of particles are shown. Primary mouse thymocytes were induced to undergo apoptosis by dexamethasone (dex) treatment in all indicated experiments.
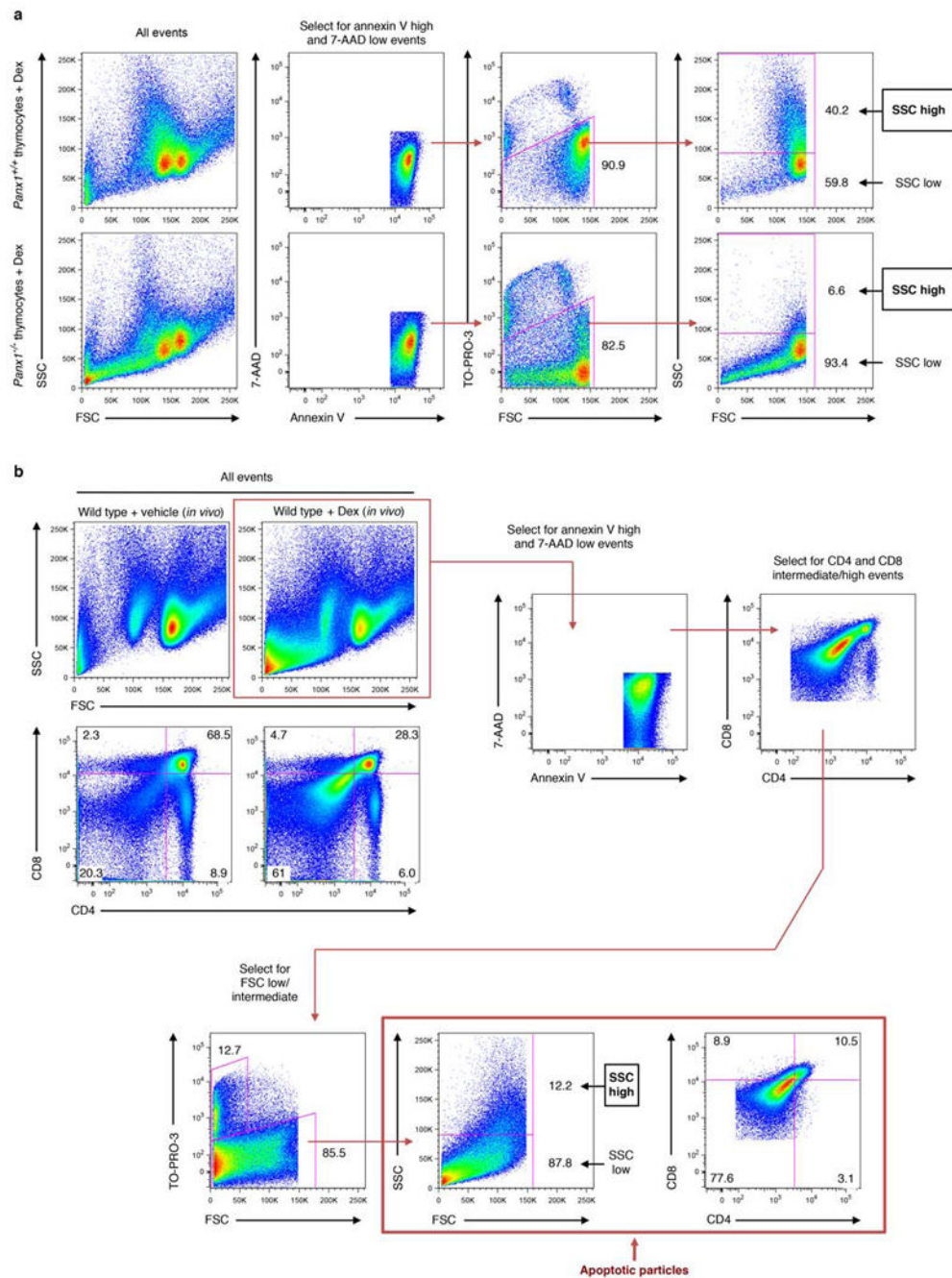
Extended Data Figure 6. Electronic gating strategy for analysing the complexity of subcellular apoptotic particles generated *ex vivo* and *in vivo*

a, Flow cytometry analysis showing electronic gating strategy used to distinguish annexin V[high], 7-AAD[low] subcellular particles generated from primary mouse thymocytes induced to undergo apoptosis via dexamethasone treatment. Subcellular apoptotic particles with high complexity (SSC high) or low complexity (SSC low) are gated as shown. **b**, Flow cytometry analysis showing electronic gating strategy used to distinguish different subsets of apoptotic cell-derived particles generated in the thymus of mice injected intraperitoneally with
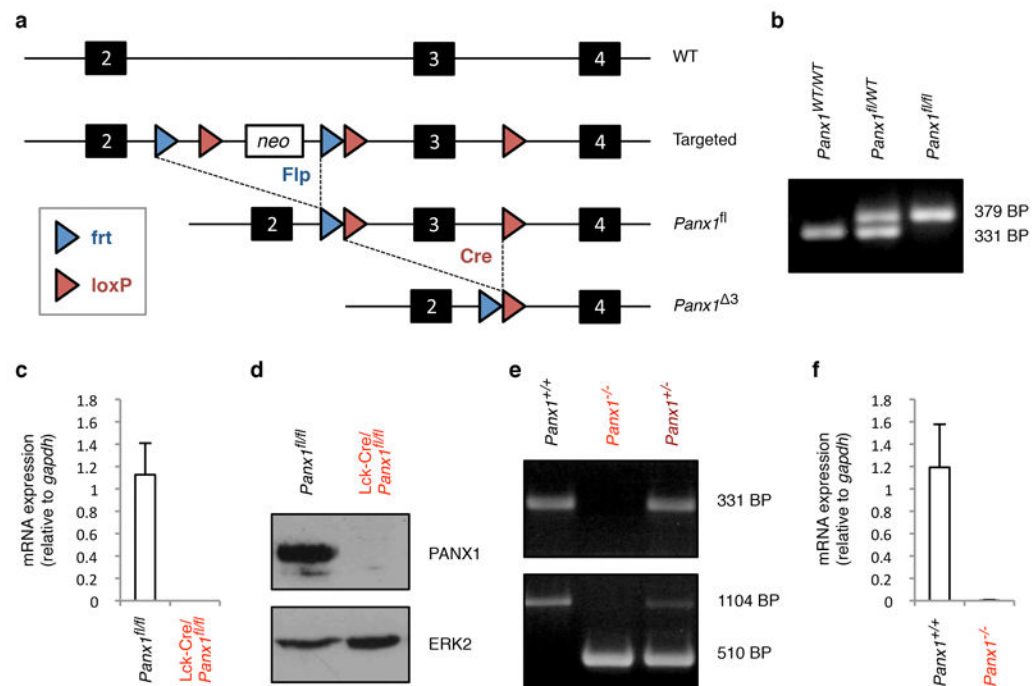
dexamethasone (6 h). Annexin V^{high}, 7-AAD^{low}, CD4/CD8^{intermediate} particles were initially selected and subsequently gated based on forward scatter (FSC, indicative of cell size). Apoptotic particles of interest (as indicated) are therefore defined as Annexin V^{high}, 7-AAD^{low}, CD4/CD8^{intermediate} and FSC$^{low/intermediate}$.

Extended Data Figure 7. Generation of conditional and global pannexin 1 deficient mice
a, Strategy for deletion of neomycin cassette and exon 3 of *Panx1*. **b**, Identification of mice with floxed *Panx1* loci, assessed by PCR. **c**, mRNA levels of *Panx1* in CD4+ thymocytes relative to *Gapdh*. n = 3 mice per group. **d**, Immunoblotting of lysates from thymocytes with the indicated genotypes. **e**, Identification of mice with wild-type, heterozygous and homozygous *Panx1* targeted loci, assessed by PCR. **f**, mRNA levels of *Panx1* in thymocytes with the indicated genotypes relative to *Gapdh*. n = 3 mice per group. Error bars in **c** and **f** represent s.e.m.
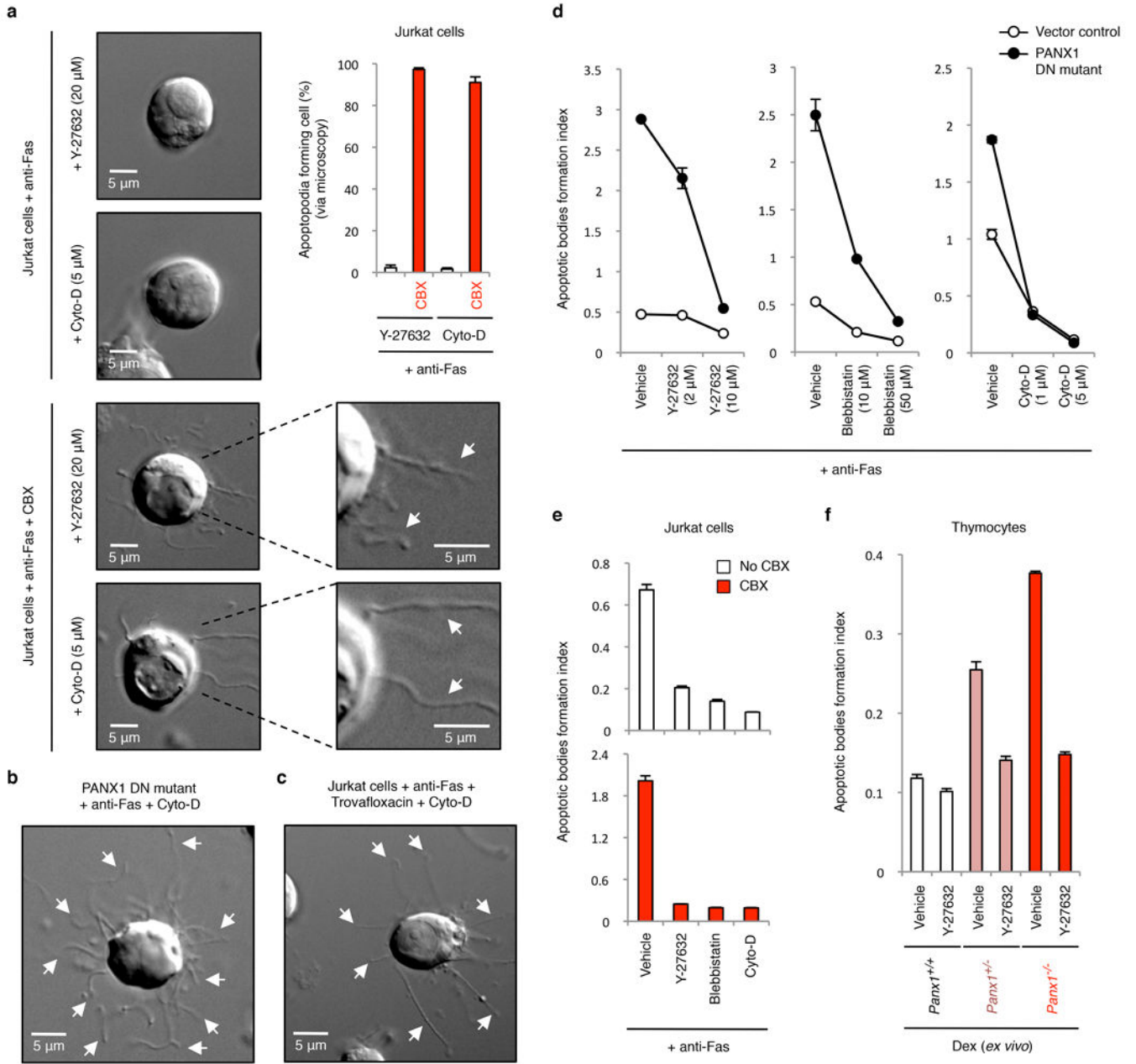
Extended Data Figure 8. Formation of apoptotic bodies but not string-like apoptopodia structures is dependent on actomyosin contraction

a, Time-lapse images monitoring apoptotic cell morphology of cells treated with or without CBX (500 μM) and in the presence of actomyosin contraction inhibitors. Top right, percentage of apoptotic cells forming string-like apoptopodia structures (387, 414, 459 and 372 apoptotic cells were analysed for Y-27632, Y-27632+CBX, Cyto-D and Cyto-D+CBX-treated cells, respectively, from three independent experiments). **b,c**, Time-lapse images monitoring apoptotic cell morphology of cells stably expressing the dominant-negative PANX1 mutant (PANX DN mutant) (**b**) or treated with 40 μM trovafloxacin (**c**) in the presence of Cyto-D (5 μM). **d**, Inhibitors of blebbing, Y-27632, blebbistatin, or cytochalasin

D (Cyto-D) reduce the formation of apoptotic bodies in Jurkat cells expressing PANX1 DN mutant (n=3). **e**, Generation of apoptotic bodies by dying cells treated with Y-27632 (10 μM), blebbistatin (50 μM) and Cyto-D (5 μM). Cells were induced to undergo apoptosis in the presence or absence of CBX (500 μM) (n=3). **f**, The enhanced formation of apoptotic bodies in apoptotic thymocytes from mice with PANX1 deficiency is also blunted by the ROCK inhibitor Y-27632 (10 μM) that blocks membrane blebbing (n=3). Error bars represent s.e.m. Scale bars represent 5 μm. Arrows, apoptopodia.
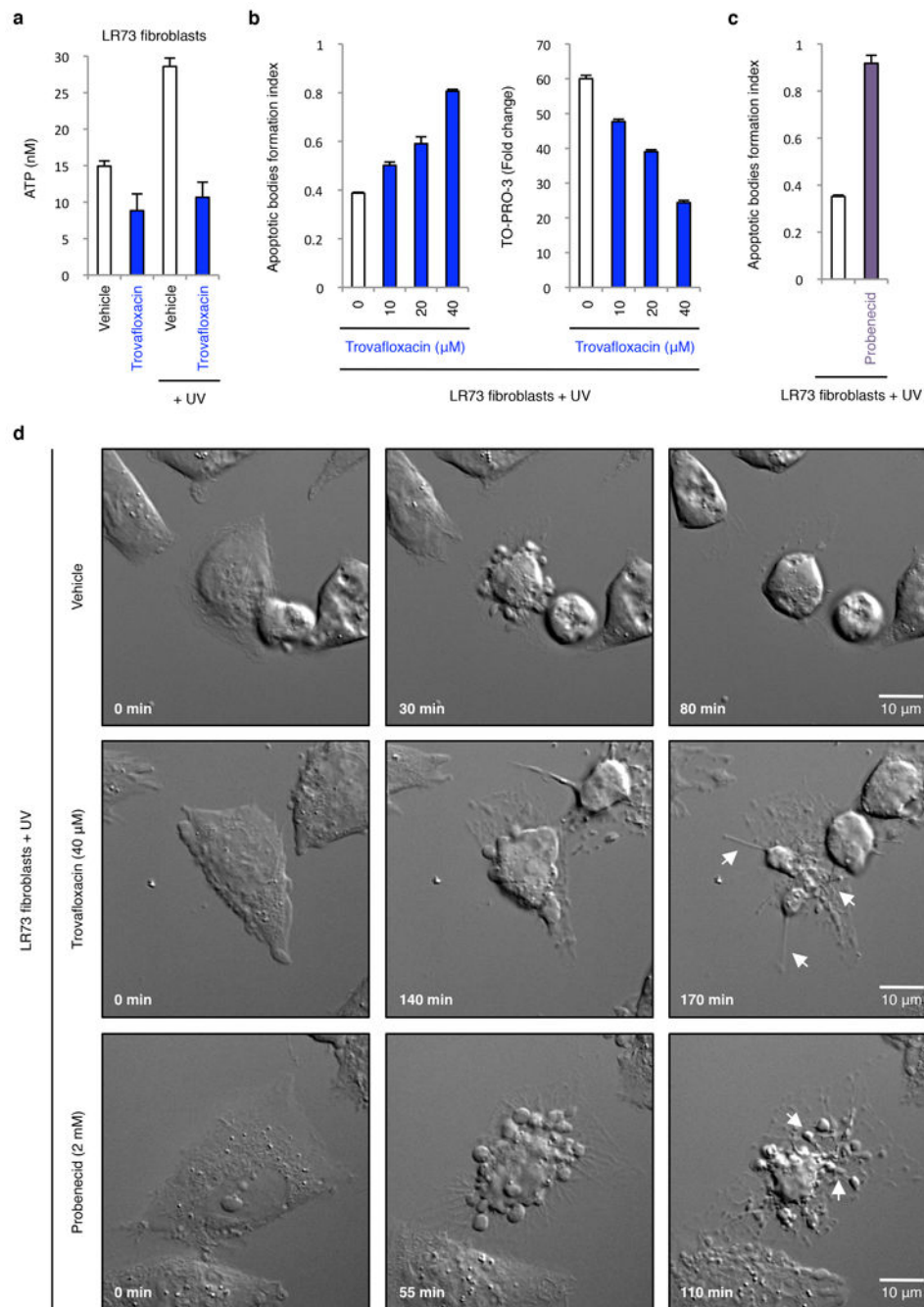
Extended Data Figure 9. Inhibition of pannexin 1 during UV-induced apoptosis in LR73 fibroblasts promotes the formation of membrane protrusions and apoptotic bodies

a, ATP levels in supernatants of LR73 fibroblasts treated with 40 μM trovafloxacin with or without apoptosis induction (*n*=3). **b**, Formation of apoptotic bodies (left) and TO-PRO-3 uptake (right) by LR73 fibroblasts treated with the indicated concentrations of trovafloxacin (*n*=3). **c**, Generation of apoptotic bodies by LR73 fibroblasts treated with 2 mM probenecid (*n*=3). **d**, Time-lapse images monitoring apoptotic cell morphology of LR73 fibroblasts treated with or without trovafloxacin (40 μM) or probenecid (2 mM). LR73 fibroblasts were
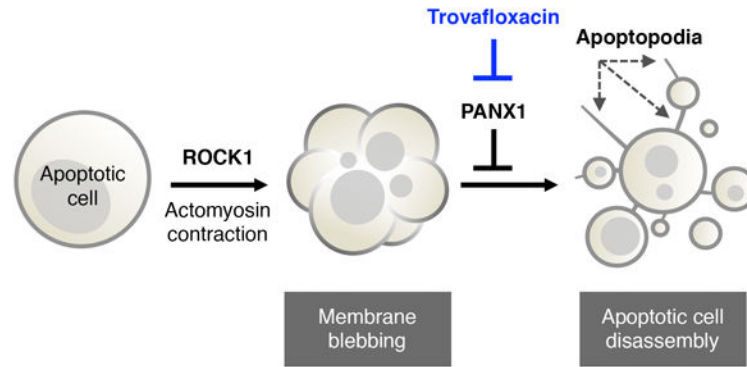
induced to undergo apoptosis by UV treatment in all indicated experiments. Error bars in **a-c** represent s.e.m. Arrows, apoptopodia. Scale bars represent 10 μm.

Extended Data Figure 10. Schematic diagram depicting where pannexin 1 likely acts in limiting the fragmentation of apoptotic cells

Blocking PANX1 function (for example via trovafloxacin) leads to formation of apoptopodia, and subsequently the release of apoptotic bodies.